Volume 2, Issue 4, 2024

Frontier in Medical & Health Research

ISSN: (e) 3007-1607 (p) 3007-1593

ANTIBACTERIAL AND PHOTO-CATALYTIC APPLICATIONS OF BIO-INSPIRED EUPHORBIA PROSTRATA-MEDIATED IRON NANOPARTICLES

Salman[1], Arshad Islam[*2,3], Muhammad Qasim[4], Asad Zia[5], Ajmal Khan[1], Farhan Ahmad[*1]

[1]*Institute of Biotechnology and Microbiology, Bacha Khan University, Charsadda, Khyber Pakhtunkhwa, 24420 Pakistan.*

[2]*Sulaiman Bin Abdullah Aba Al Khail Centre for Interdisciplinary Research in Basic Sciences (SA-CIRBS), International Islamic University, Islamabad, Pakistan. A.I.*

[3]*Deparmtent of Pathology, Lady Rading Hospital Medical Teaching Institution, Peshawar, Pakistan*

[4]*Department of Zoology, Faculty of Biological Sciences, Quaid-i-Azam University, Islamabad, Pakistan*

[5]*Public Health Reference Laboratory, Khyber Medical University, Peshawar, Pakistan.*

[*2]arshad.cgl@gmail.com,[*6]ahmadfarhan31@gmail.com

DOI: https://doi.org/10.5281/zenodo.17141566

Keywords
Biosynthesized iron nanoparticles, antibacterial, hemolytic assay, Euphorbia prostrata, Photo-catalytic activities

Article History
Received: 03 September 2024
Accepted: 16 October 2024
Published: 13 November 2024

Corresponding Author: *
Arshad Islam
Farhan Ahmad

Abstract

The synthesis of nanoparticles using plant extracts is a more cost-effective and environmentally friendly option than the traditional chemical or physical methods. In the current study, we synthesized iron oxide (FeO) nanoparticles (NPs) using a green approach by employing an extract from the Euphoria prostrata plant. X-ray diffraction (XRD) analysis of FeO NPs revealed its highly crystalline structure, while scanning electron microscopy (SEM), showed the agglomerated form of the particles. Energy Dispersive X-Ray (EDX) verified the elemental composition of FeO NPs and indicated their purity. FTIR spectroscopy was utilized to identify the functional groups. UV- visible spectrometry was used for the evaluation of synthesis. About 30.1% weight loss was observed in heating the sample from 25°C to 600°C. FeO NPs exhibited strong antibacterial activity, as evidenced by the development of a broad inhibitory zone (how much was the zone in mm?). FeO NPs exhibited superior antimicrobial efficacy against Pseudomonas aeruginosa, with amoxicillin as control. According to the results of a flow cytometric susceptibility test, FeO nanoparticles were able to destroy P. aeruginosa (74.12%), E. coli (72.1%), and S. aureus (62.41%) at a concentration of 400 µg/ml. The photo catalytic activity was investigated against Methylene blue and Phenol red dyes. It was noticed that 27% of the dye was damaged in the first 30 minutes; however, as the irradiation period was increased up to 150 minutes, the percentage of dye degraded reached 91.1%. Additionally, the biocompatible nature of FeO NPs was also tested which showed comparable hemolytic action than Triton X-100.

INTRODUCTION

Nanotechnology has made significant advances in the last 20 years. It is now one of the most researched and fastest-growing fields because it can be used in many areas of human welfare. Nanoparticles (NPs) are very small particles with sizes between 1 and 100 nm that can be made or found in nature. They have physical and chemical properties that are unique and valuable. At the nanoscale, the magnetic, electrical, mechanical, optical, chemical, and biological properties of

Frontier in Medical & Health Research

ISSN: (e) 3007-1607 (p) 3007-1593

particles are better. Because NPs have more surface area than volume, they are more reactive, mobile, dissolve easily, and strong [1, 2]. In the wide variety of nanoparticles, ferric oxide nanoparticles (FeONPs) stand out as one of the most significant type of metal oxide nanoparticles. These nanoparticles are notable for their magnetic properties as well as their compatibility with living organisms [3]. Based on their size, distribution, and structure Iron Oxide has applications in numerous fields, including antimicrobial [4], mosquitocidal [5], anti-plasmodial [6], larvicidal [7], ovicidal and larvicidal potential for malaria, dengue, and filariasis mosquito vectors [8]. Iron oxide nanoparticles with suitable surface chemistry are used in immunoassay, tissue repair, detoxification of biological fluids, cell sorting, and hyperthermia [9], targeted drug delivery [10], and cancer [11]. In addition, it was used as inhibitors for dengue growth [12]. FeO NPs are considered the most promising agent for all the above functions.The development of antibiotic-resistant strains is a major concern for the wellbeing of people all over the world. The antibacterial activity of iron oxide nanoparticles (FeO NPs) is receiving a great deal of attention. Different types of bacteria have been utilized for the bactericidal activity of FeO NPs [13]. Iron Oxide NPs can be used in regenerative medicine [14] due to the fact that these NPs have good biocompatibility in vivo and in vitro [15, 16]. This is something that sets it apart from ZnO NPs on a fundamental level. FeO NPs are a desirable contender for the role of an antibacterial preparation of the next generation as a result of their antimicrobial activity as well as their compatibility with living organisms [17, 18]. The production of Iron Oxide NPs and the improvement of its effectiveness have been accomplished through the application of a wide variety of chemical and physical techniques. The sol-gel process, co-precipitation, microemulsion, hydrothermal, chemical vapor deposition, and polyol are the most common chemical processes used in the formation of nanoparticles. In the process known as metal reduction, a reducing agent is applied to a solution that already contains a metal ion. For the synthesis of NPs, the majority of the time, reducing agents consisting of $NaBH_4$, sodium citrate, ascorbic acid, and hydrazine are utilized. However, there are some instances in which a stabilizing agent may be necessary [19, 20]. However, these traditional methods use chemicals that are both expensive and hazardous, and as a result, they cannot be termed an environmentally friendly approach [21, 22]. Taking into consideration, researchers in today's world have shown a great deal of interest in the synthesis of metal and metal oxide NPs through the use of green synthesis [23]. The twelve primary systems of green chemistry can be utilized to determine the technique for green synthesis. The biogenic system of nanoparticles is one method that is frequently utilized [24]. When compared to conventional synthesis methods, the utilization of microorganisms (fungi and bacteria) [25] as well as natural products (fruit juice, polysaccharides, and plant extracts) containing plentiful hydrogen atoms for the biosynthesis of nanoparticles is more advantageous. This is the case in terms of biocompatibility, low production expenses, and a natural reductive chemical atmosphere [26, 27]. In addition, plant extracts that contain reducing and stabilizing agents offer a biological route for the synthesis of metallic NPs that does not involve the use of toxic organic solvents. This paves the way for a controlled synthesis that results in highly ordered NPs of any size, shape, and dispersion [28]. Furthermore, the typical reduction potential of these phyto-compounds is around 0.534 V, whereas the reduction potential of metallic iron is 0.44 V. Since the reduction process is spontaneous, the phyto-compounds surround the nanoparticles, which provides stability and a distinctive form [29, 30]. Among different plants the annual herb *Euphorbia prostrata* is characterized by its prostrate growth habit, hirsute pubescence, and widespread distribution across Asia. Antibacterial, nematicidal, and antiparasitic properties can be found in extracts of the leaves of the *E. prostrata* plant. The leaf extract of *E. prostrata* has been shown to contain flavonoids, anthraquinone, phenols, phlobatannins, polysaccharides, saponins, tannins, and terpenoid [31, 32]. Keeping in view the benefits of green synthesis over traditional techniques a study was designed to synthesize FeO NPs using *E. prostrate* leaf extract. Evaluation of the synthesized NPs's therapeutic applications were among the study objectives.

Frontier in Medical & Health Research

ISSN: (e) 3007-1607 (p) 3007-1593

Materials and methods

2.1 Plant material collection and extract preparation

The *Euphorbia prostrata* plant was collected in Charsadda, Khyber Pakhtunkhwa. Fresh plant material was employed in the synthesis of FeO NPs.

2.2 Materials / Chemicals

In this investigation, all the chemicals like nutrient agar, nutrient broth, iron chloride etc. were of high degree purity and were purchased from Sigma Aldrich®.

2.3 Preparation of plant extract

Euphorbia prostrata plant was cleaned three times with distilled water. About 50g of fresh plant was chopped into small pieces and ground by morter-pestal before being mixed to 200 ml of de-ionized water in a flask and stirred for 15 min. The extract was filtered, cooled to ambient temperature, and kept at – 4°C for future use.

2.4 Preparation of FeONPs

Iron oxide nanoparticles were synthesized by modified protocol from the previous studies [33]. Briefly, one millimolar (1mM) iron chloride solution was added to *Euphorbia prostrata* plant extract in a 1:2 volume ratio and placed on the magnetic stirrer for one hour to examine the reaction mixture's color. FeO nanoparticles were synthesized when dark brown color turned black. The above approach was used to produce FeO NPs for further characterization after the confirmation test.

2.5 Characterizations of iron oxide nanoparticles

Characterization procedures let us quickly and accurately grasp the properties of the substance or nanoparticles being researched. UV–Vis spectrophotometers confirmed FeO NP production (Shimadzu UV 2450). Fourier transform infrared spectrophotometers evaluated FeO NPs' functional group. SEM, XRD, and EDX measured FeO NP size, shape, and elemental composition.

2.6 Antibacterial activity

Well Diffusion assays were used to test the antibacterial efficacy of plant-mediated produced FeO NPs against a range of gram-positive and gram-negative bacteria. Bacterial cultures were disseminated onto nutrient agar (NA) plates using a sterile spreader. By using a borer, wells were drilled into the agar-filled plates. FeO nanoparticle solutions of varying concentrations were poured into the wells. A 24-hour incubation period at 37°C was performed after the plates were set in place. Measurements of inhibitory zones were taken after a 24-hour incubation period [34].

2.7 Efflux pumps inhibition (Cart wheel assays)

To investigate the efflux inhibitory effect of iron oxide nanoparticles, Cartwheel assay was performed on different bacterial strain. In cartwheel assay, bacteria eject ethidium bromide (EtBr), which is a conjoint substrate for many efflux pumps (transporter proteins) were used. Within the cells, Efflux pumps inhibitors (EPI) leads to deposit of EtBr and generate fluorescence. EtBr and nanoparticles were taken in different concentration in each micro centrifuge tube. MDR strains were swabbed in TSA plates containing different concentrations of EtBr and incubated for 16 hours at 37°C. For control, bacterial strains and EtBr without NPs was swabbed on nutrient agar plates in cartwheel pattern. The plates were incubated for 24 hours at 37°C. After incubation the plates were detected for fluorescence under UV transilluminator [35].

2.8 Bacterial cell membrane damage assay

By measuring the absorbance of intracellular substance generated when nanoparticles interact with cell, researchers were able to examine the impact of nanoparticles on membrane integrity. The inoculum for the bacteria was grown by transferring a loopful of culture from the nutrient agar plate to the nutrient broth and incubating it at 37°C for a full 24 hours. The culture was harvested, washed, and resuspended in PBS solutions following centrifugation at 10000rpm for 10 minutes. In the end, the 420 nm absorbance of the solution was adjusted to 0.7. The bacterial inoculum was combined with 1.5 mL of NPs at

Frontier in Medical & Health Research

ISSN: (e) 3007-1607 (p) 3007-1593

varying concentrations. Shimadzu UV 160 UV-visible spectrophotometer readings were taken at 260 nm to determine the rate of intracellular substance release [36].

2.9 RBC Hemolytic assay

Hemolysis is defined as the breaking of the erythrocyte membrane in order to release haemoglobin into the plasma. The previous approach, with minor modifications, was used to perform hemolytic activity against iron oxide nanoparticles. A syringe was used to take blood from a healthy volunteer male person. To suppress blood coagulation, 5 mL of blood was placed in an EDTA tube. Blood was centrifuged for 5 minutes at 3000 rpm. The RBC pellet was resuspended in 10 mL pH 7.4 PBS after removing the platelet-depleted plasma supernatant. The buffy RBC layer was removed twice or three times. For a uniform cell suspension, PBS was added [37]. The experiment was carried out in dark. Iron oxide NPs at various concentrations were added to Eppendorf tubes with diluted blood. Triton X-100 and PBS were incubated for 3 hours at 37 °C. 1500 rpm centrifuged suspended cells for 15 minutes. Carefully collecting the supernatant, the absorbance at 576 nm was measured.

2.10 Photocatalytic study

The photo catalytic experiment used 20ppm methylene blue dye in 50ml deionized water. The standard solution was separated, and 0.02g of biosynthesized FeO NPs catalyst was added to the leftover (45 ml) solution. After 30 minutes in the dark to reach adsorption-desorption equilibrium, the UV lamp was turned on and 5ml was removed every 30 minutes using a small syringe. Centrifugation at 12000 rpm for 10 minutes separated the NPs from the dye solution, and a UV-Visible Spectrophotometer evaluated their absorption [38]. Lambda max of the dye was 662 nm. The procedure below estimated the dye degradation percentage.

$$\text{Degradation (\%)} = \frac{Ao - At}{Ao} \times 100 \ldots (1)$$

"*At*" is the time interval and "*Ao*" is the initial concentration of dye

Results

3.1 Optical properties of FeO NPs.

UV-visible spectroscopy was used to determine the optical characteristics of FeO nanoparticles. Shimadzu UV-1800, Japan, was used to evaluate the absorption spectra of FeO nanoparticles. The optical absorption value was measured in the wavelength range of 200 to 800nm. At 260nm(Figure 1), optical absorption was found for the synthesized FeO nanoparticles utilizing *Euphoria prostrata*.

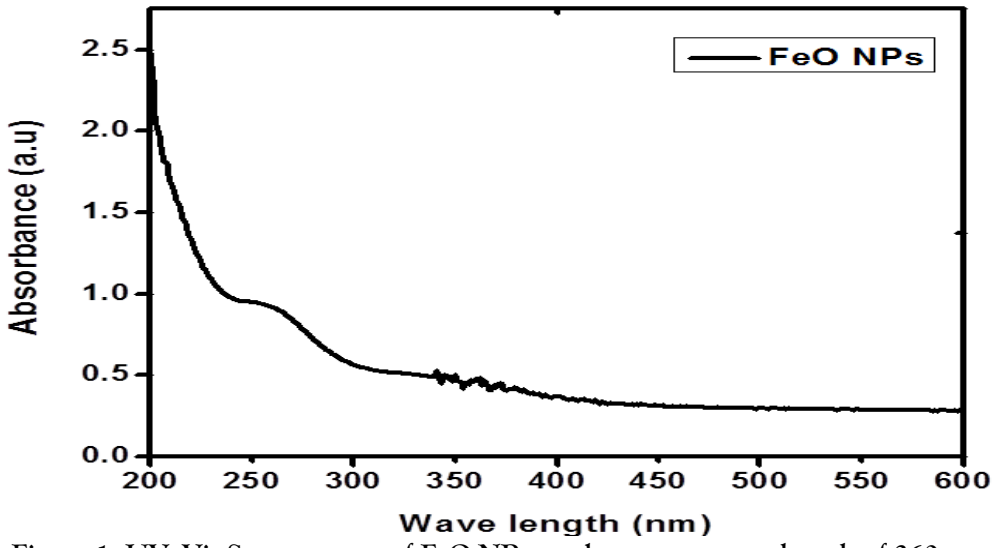

Figure 1. UV- Vis Spectroscopy of FeO NPs, peak appear at wavelength of 260 nm

3.2 FTIR analysis

FTIR study shows biomolecules in *Euphorbia prostrata's* aqueous extract that may cap and

Frontier in Medical & Health Research

ISSN: (e) 3007-1607 (p) 3007-1593

reduce Fe^{+2} ions. The FTIR spectra of the *Euphorbia prostrata* aqueous extract showed prominent bands at 1040, 1632 and 3324 cm^{-1}, while that of iron oxide nanoparticles showed wide peaks at 540,1100, 1650, and 3434 cm^{-1}(Figure 2). The O-H stretching vibration of polyphenols causes the extensive peak at 3324 cm^{-1} in *Euphorbia prostrata* plant extract and 3434 cm^{-1} in FeO NPs. The large peaks at 1650 and 1632 cm^{-1} in *Euphorbia prostrata* plant extract and FeO nanoparticles, respectively, are connected to carbonyl C=O groups, while the absorption band at 1100 cm^{-1} in iron oxide nanoparticles is due to O-H bending and C-H starching vibration. FeO stretching may cause the peak at 540cm^{-1}.

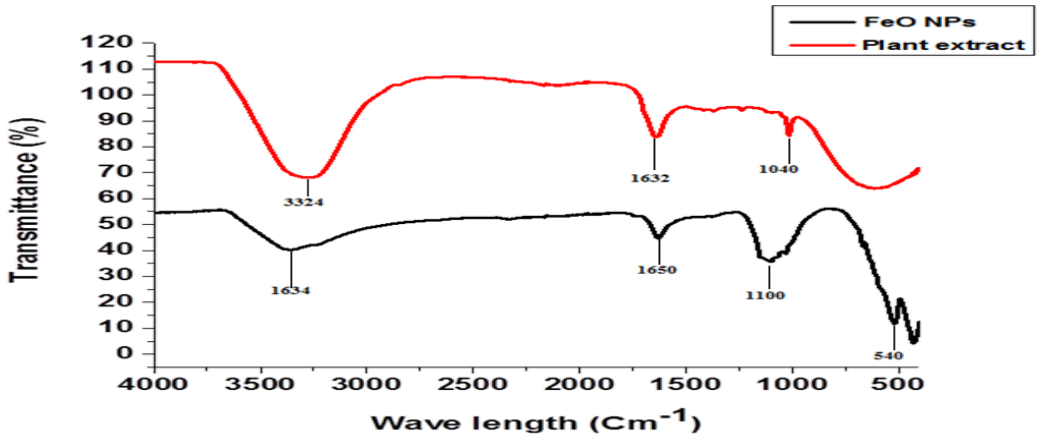

Figure 2 FTIR analysis of FeO NPs and Euphorbia prostrata extract

3.3 SEM analysis

SEM examination was used to determine the structure and morphology of FeO NPs, which showed that the size of these nanomaterials was 25 and 55 nm. The produced particles were agglomerated and posed various sizes (Figure 3). The occurrence of natural substances on the particle surface caused the agglomeration of nanoparticles. As a result of H-bonding between bioactive chemicals, the particles had a tendency to agglomerate.

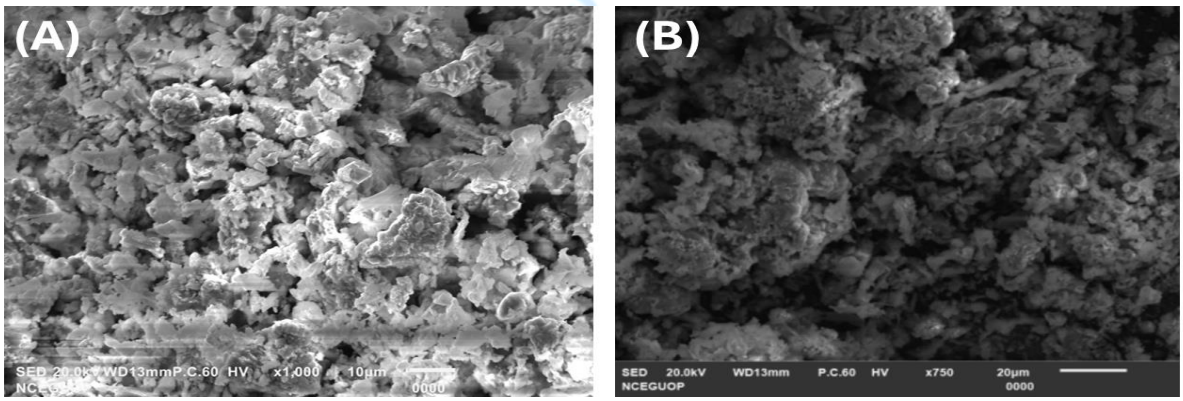

Figure 3. SEM images of FeO nanoparticles at scale of 10 and 20 µm

3.4 XRD analysis

The crystal nature of the prepared FeO nanomaterials was investigated by X-ray diffraction, as demonstrated in (Figure 4). Exact peaks of diffraction were seen at 2 thetas = 63.99, 62.41, 57.59, 54.09, 49.48, 35.61, 30.85, 24.13 and 33.15, corresponded to the planes (300), (018), (214), (116), (024), (110) (113), (012) and (104), Bragg considerations and validate the rhombohedral phase of FeO NPs. These XRD results closely match the card (JCPDS; 33-0664) and no other impurity peaks have been observed. The XRD examination demonstrated the materials' purity and crystallinity. Using the Debye-Scherrer equation, the crystallite size is calculated.

Frontier in Medical & Health Research

ISSN: (e) 3007-1607 (p) 3007-1593

$$D = k\lambda/\beta\cos(\theta) \ldots (2)$$

The aforementioned equation was utilized to calculate the mean size of crystallites.

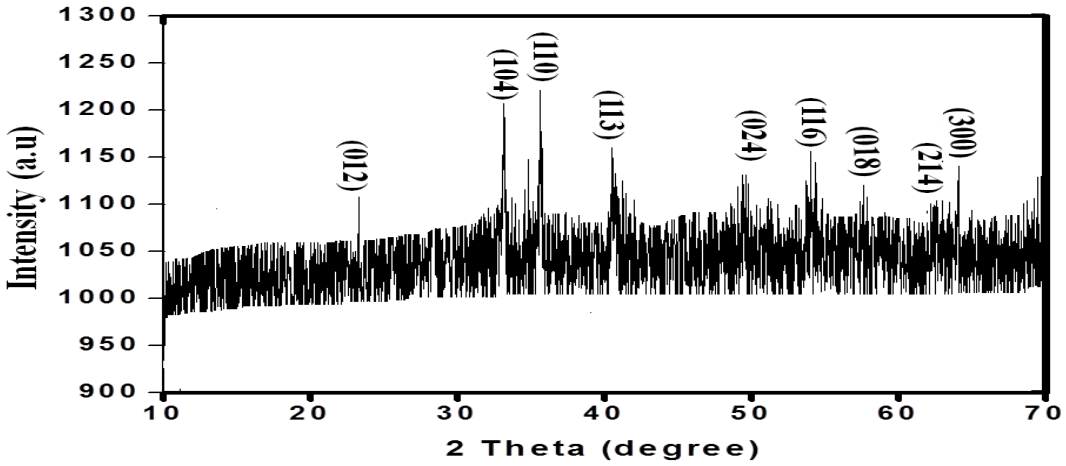

Figure 4. XRD analysis of FeO nanomaterials synthesized from *Euphorbia prostrata* plant extract

3.5 EDX analysis

The EDX spectrum of the synthesized FeO NPs is depicted in (Figure 5). The elemental composition analysis of the biosynthesized FeO NPs revealed the existence of oxygen (O) and iron (Fe) in the sample and demonstrates their great purity. 30.96% and 25.65% of the produced FeO NPs are composed of iron (Fe) and oxygen (O), respectively. This is comparable to the percentage of theoretically probable stoichiometric mass. The presence of Zn,Ca,Si, K, and Mg suggests the existence of plant constituents covering the FeO NPs.

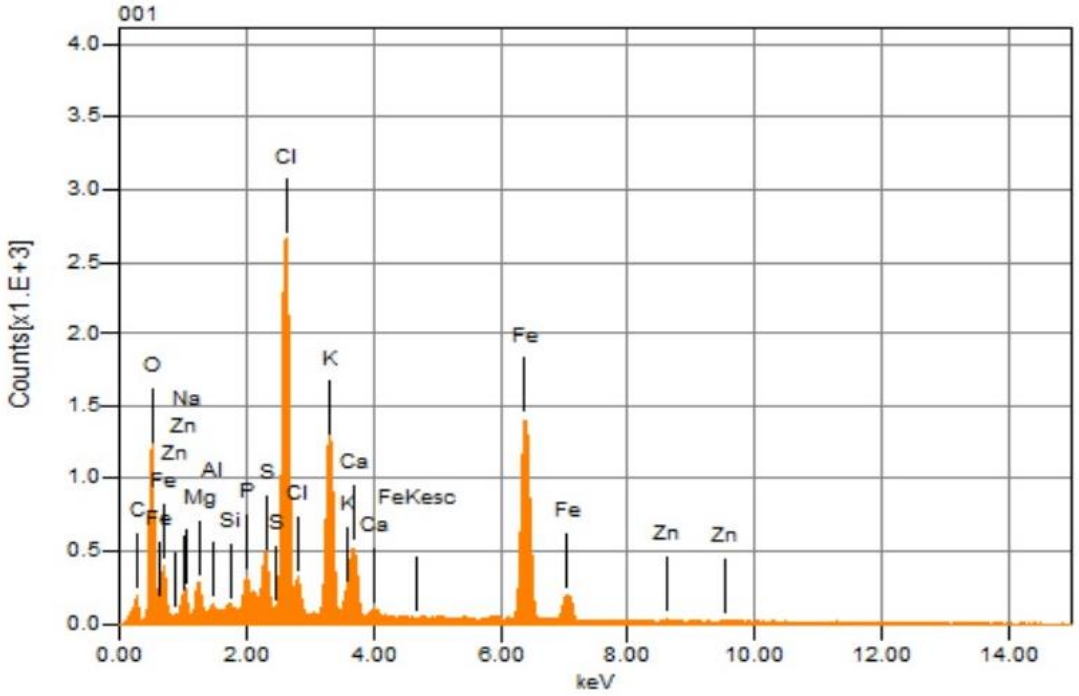

Figure 5: EDX spectra of the biosynthesizedFeONPs.

Frontier in Medical & Health Research

ISSN: (e) 3007-1607 (p) 3007-1593

3.6 TGA analysis

Thermo gravimetric analysis of FeO nanoparticles is shown in Figure 6. The weight loss of the produced substance was measured in air at a breakdown rate of 15 °C/min. Prepared sample experienced 30.1% weight loss from 25 to 600°C temperature.

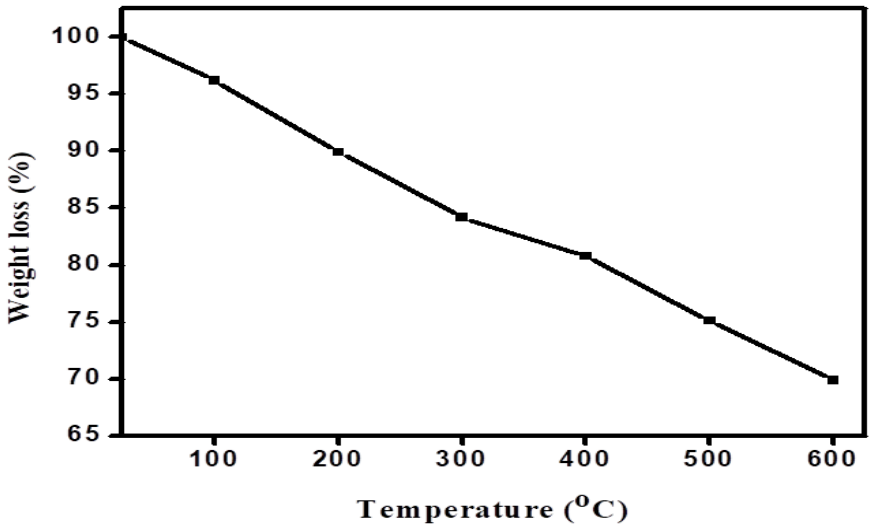

Figure 6: TGA analysis of FeO nanoparticles

3.7 Antibacterial activity

Well diffusion technique was used to examine the antibacterial properties of iron oxide NPs against a variety of harmful bacteria. Creating a sizable zone of inhibition demonstrates effective antibacterial action, which was confirmed for the FeO NPs. Improved antimicrobial activity of FeO NPs was shown against a variety of pathogenic bacterial strains, including *P. vulgaris*, *P. aeruginosa*, *E. coli*, and *S. aureus*, as demonstrated in (Figure 7aand b). It was shown that FeO NPs had significant bactericidal action than the standard medication amoxicillin. Factors such as cell wall impermeability, concentration, bacterial species, physicochemical qualities, and ribosome variation all have a role in how well FeO nanoparticles kill different types of bacteria.

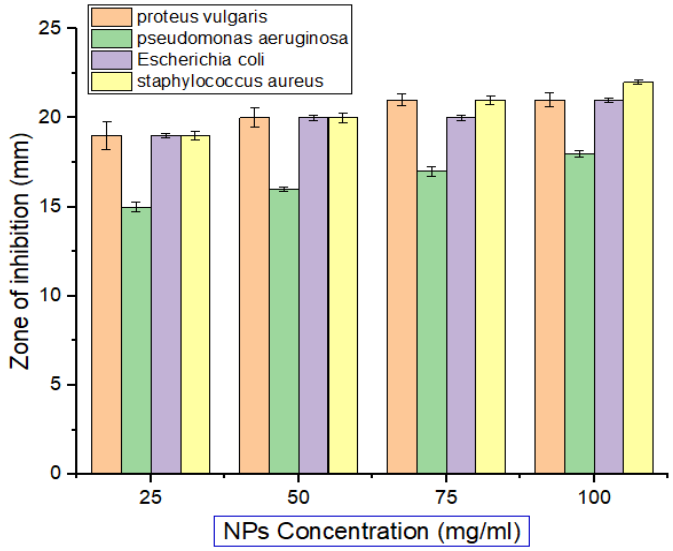

Figure 7a: Antibacterial activity of FeO nanoparticles at various concentrations

Frontier in Medical & Health Research

ISSN: (e) 3007-1607 (p) 3007-1593

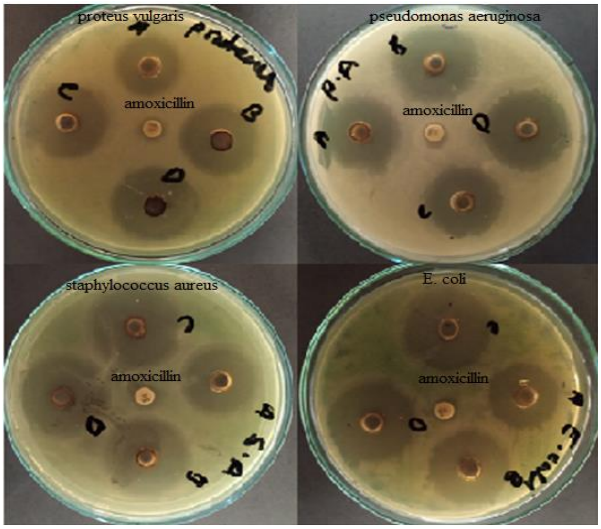

Figure 7b: Bacterial zone of inhibition of FeO nanoparticles

Table 1. Bacterial cell membrane damaged

Concentrations (µg/ml)	(*E. coli* % damage)	Cell membrane damage (*Pseudomonas*% damage)	(*Staphylococcus* % damage)
400	72.1±0.93	62.41±0.89	74.12±0.28
200	62.37±0.28	53.51±0.85	63.63±0.39
100	51.86±0.73	45.23±0.22	53.64±0.56
50	33.29±0.66	27.76±0.55	42.47±0.26
25	21.16±0.24	19.41±0.35	32.39±0.15

Table1 shows that at 25, 50, 100, 200, and 400 µg/ml, the cell viability of *E. coli* was reduced by 21.16±0.24%, 33.29±0.66%, 51.86±0.73%, 62.37±0.28%, and 72.1±0.93%, respectively. At the same concentrations (25, 50, 100, 200, and 400 µg/ml) FeO NPs caused 19.41± 0.35%, 27.76 ±0.55%, 45.23±0.22%, 53.51±0.85%, and 53.64±0.56% of cell membrane damage in *Pseudomonas aeruginosa*, respectively. At 25 µg/ml, *Staphylococcus aureus* cell membrane damage is 32.39±0.15%, at 50 µg/mL, its 42.47±0.26%, and at 100 µg/ml, its 74.12±0.28%. According to a flow cytometric susceptibility test, at 400 µg/m1, iron oxide nanoparticles killed 72.1% of *E. coli* cells, 62.4% of *Staphylococcus aureus* cells, and 74.12% of *Pseudomonas aeruginosa* cells, respectively. It could be because FeO NPs invade the bacterial cell, where they function as a bactericidal or bacteriostatic agent, preventing the bacterium from growing and multiplying.

3.8 Efflux Pump Inhibition Assay/Cart Wheel Assay

This straightforward technique is based on the fact that many efflux pumps require ethidium bromide (EtBr) as a substrate. As a result of efflux pump inhibitor accumulation, EtBr causes blooming at significantly lower concentrations. An evaluation of iron oxide NPs' efflux inhibitory impact using a cart wheel experiment was carried out(Figure 8). We performed cartwheel assay for *Pseudomonas aeruginosa*,*Staphylococcus aureus, E coli, Citrobacter freundii, Klebsiella penumoniae*, and *proteous vulgaris* by incorporating 2, 4, 6, 8, 10, and 12mg/ml of iron oxide NPs in the agar media and evaluating the fluorescence exhibited by EtBr in all the bacteria tested. Treatment without FeONPs was maintained as control.

Frontier in Medical & Health Research

ISSN: (e) 3007-1607 (p) 3007-1593

inhibition of ion exchang channels by green synthesized iron oxide nanoparticles from *euprobia prostrata* plant extract

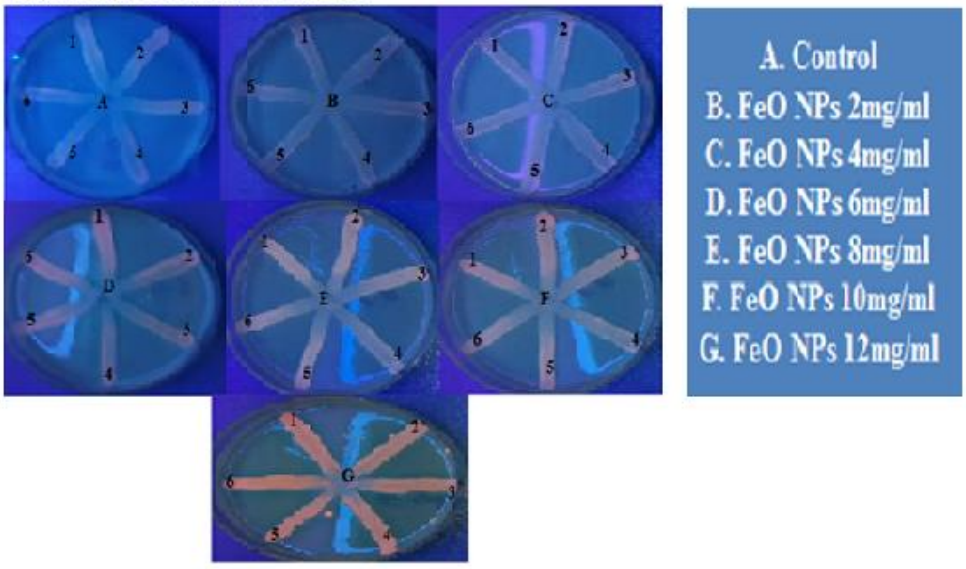

1.Ecoli, 2.stapylococcuse aureus, 3.pseudomonas aeruginosa, 4.citrobacter freundii, 5. klebsiella pneumoniae, 6.proteous vulgaris, 7.

Figure 8. Cart Wheel Assay of FeO NPs

3.9 Hemolytic assay of FeO NPs

The hemolytic activity of FeO NPs at 37 °C was measured at various doses (5, 10, 15, and 20mg/ml), with triton X-100 serving as a positive control and phosphate-buffered saline (PBS) serving as a negative control (Fig. 9). Values showed that the prepared NPs had lower hemolytic activity than the positive control (triton X-100). Increased cellular permeability is the mechanism by which the NPs cause hemolysis. The cell death caused free radical generation and total cell death, which safely reduced the RBCs count.

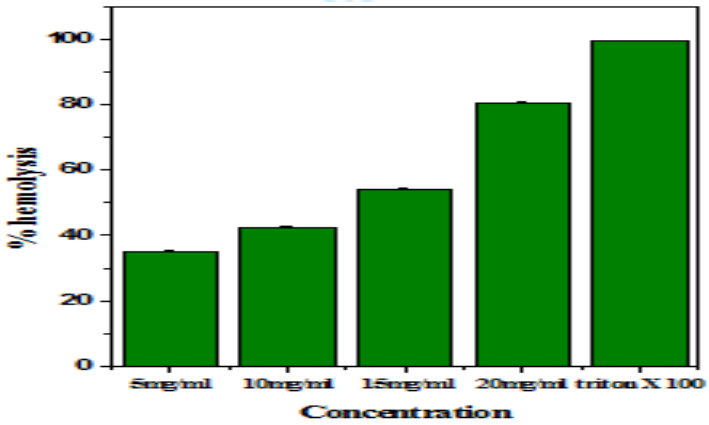

Figure 9. Hemolytic activity of FeO nanoparticles

3.10 Photocatalytic Activity

Effect of irradiation time on degradation of Methylene blue and phenol red dye

For initial 30min illumination the degradation of Methylene blue dye and Phenol red dye was27.5% and 35.8% respectively while with further increasing the time the degradation of both the dyes increased. Maximum degradation at 150min for Methylene blue dye and Phenol red dye was 91.1% and 75.02% as exhibited in figures 10 (a, b) and 11 (a, b) respectively.

Frontier in Medical & Health Research

ISSN: (e) 3007-1607 (p) 3007-1593

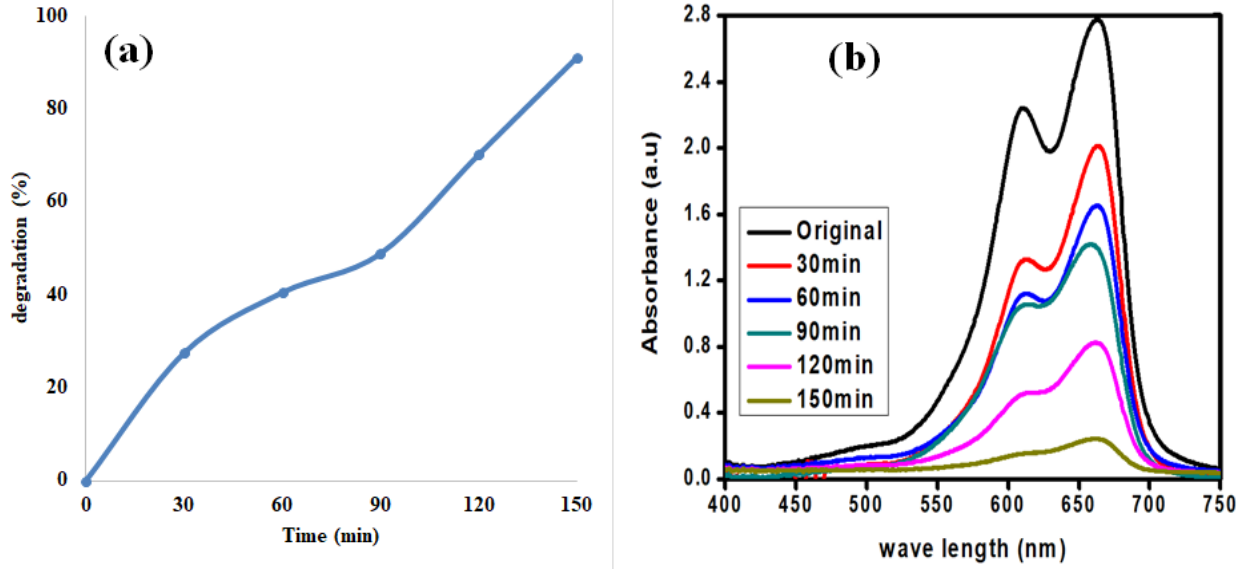

Figure 10: (a) Percent degradation of Methylene blue dye and (b) their UV-Vis Spectra by using FeO NPs.

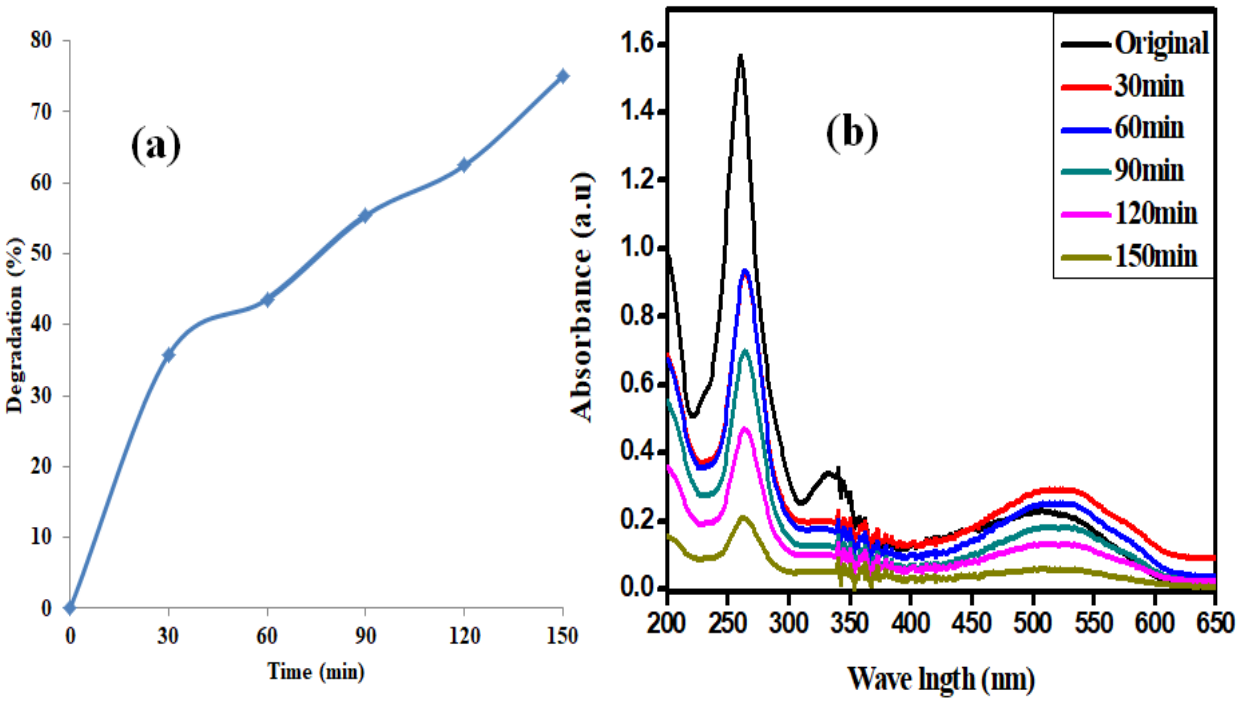

Figure 11. (a) Percent degradation of phenol red dye and (b) their UV-Vis Spectra by using FeONPs.

3.11 Photo catalytic degradation mechanism

Methylene blue and Phenol red dyes degradation could both take place by photo catalysis, as seen below: Once the photo catalyst has had the dye molecules adsorbed on its surface and been irradiated with UV light, the excitation of electrons from the valance band to the conduction band occurs, leaving holes (h+) behind in the valance band(Figure 12). After arriving at the photo catalyst's surface, the h+ and e couple will react with adsorbed water molecules, dissolved oxygen, and the surface's hydroxyl groups, resulting in the formation of hydroxyl and superoxide free radicals. As shown in scheme 1, the h+ ions react with water molecules to form •OH radicals, while the e- ions decrease the dissolved oxygen in the dye to form the superoxide anion radical O_2•. These light-generated free radicals would then

Frontier in Medical & Health Research

ISSN: (e) 3007-1607 (p) 3007-1593

be able to destroy the dye molecules, leaving behind only carbon dioxide (CO_2) and water (H_2O) [39].

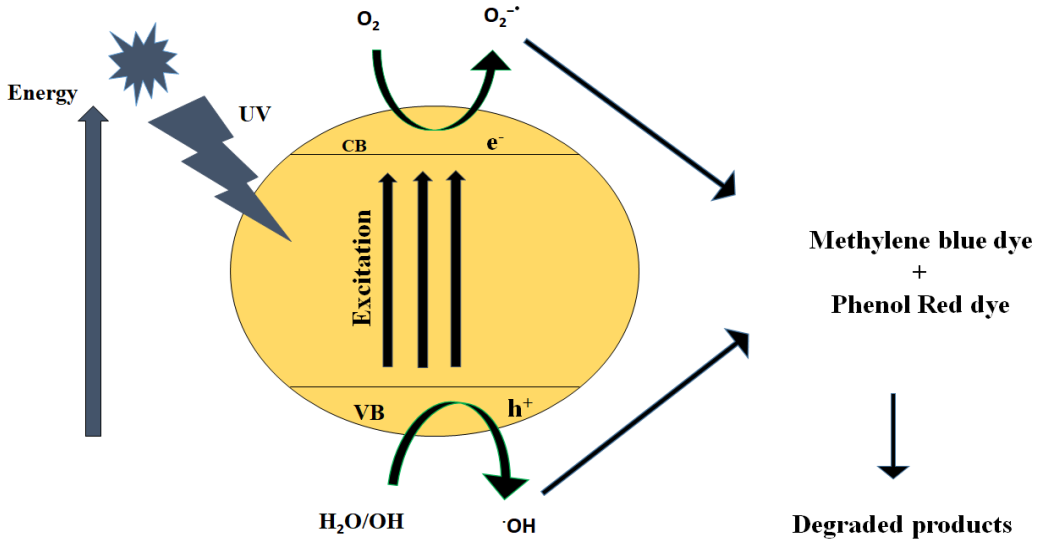

Figure 12. Possible mechanism for the degradation of Methylene blue and Phenol red dyes

FeO (NPs) +hν⟶ e^- + h^+... (3)
H_2O + h^+ ⟶·OH• + H^+... (4)
O_2 + e^-⟶· O_2•−... (5)
OH + dye⟶ degradable product... (6)
O_2^- + dye⟶ degradable product... (7)

Discussion

Due to its simplicity, nontoxicity, reduced time requirements, and low cost, as well as its potential for large-scale production, green nanotechnology has gained significant popularity in the research community in recent years. Here, we have used green synthesis to create iron oxide nanoparticles from a *Euphorbia prostrata* plant extract and evaluated their antimicrobial, hemolytic, photo catalytic, and bacterial cell membrane-damaging properties. Additionally, FeO NPs were characterized using a number of analytical techniques, including UV-visible spectroscopy, FTIR, SEM, EDX, and XRD. UV-visible spectroscopy revealed that the sample displayed a typical peak value of FeO-NPs at 260 nm for absorbed energy. Previous work also revealed comparable results, with a peak at 277 nm in the UV-visible absorption spectra of *Agrewiaoptiva* extract-mediated FeO nanoparticles [40]

The aqueous extract of the *Euphorbia prostrate* plant contains biomolecules responsible for the formation of FeO NPs, as shown by FT-IR analysis of these molecules. Iron oxide

nanoparticles have wide peaks at 540 cm, 1100, 1650 and 3434 cm^{-1}, and in their FT-IR spectra, while the plant extract exhibited prominent bands at 1040, 1632, and 3324 cm^{-1}. Figure 2 suggests that the peak at 540 cm^{-1} is caused by the FeO stretching vibration, and this finding is consistent with the results of the previous investigation [41]. Further analysis revealed that the peaks resulted from stretching vibrations of -C = O-, C-O-C, and C-O in carboxylic acid, polysaccharide, and amino acid, respectively. Previous reports have showed similar outcomes [42]

SEM micrograph of the produced FeO NPs showed agglomeration of the FeO NPs, with particle sizes ranging from 25 to 50 nm. In addition, the synthesized iron oxide-NPs had an agglomeration morphology, which is consistent with our results. However, the size of the nanoparticle in the present study was larger than in the previous study [43], which may be attributable to variations in synthesis conditions such as incubation time, temperature, handling applications, and the nature of the plant extract.

The atomic weight and elemental makeup were also determined by EDX analysis. The 6.3 keV peak in the EDX spectrum, corresponding to

Frontier in Medical & Health Research

ISSN: (e) 3007-1607 (p) 3007-1593

iron, and the 0.7 keV peak, corresponding to oxygen, were both identified in the EDX study. In this paper, we described the EDX spectra of FeO NPs synthesized through a green technique in which $FeCl_2$ serves as the starting material. According to the EDX spectra, the FeO NPs production was productive, as evidenced by the presence of prominent peaks. However, the spectra revealed additional peaks, indicating the participation of biomolecules in the plant extract's nanoparticle formation. It has been previously documented that high-purity FeO NPs exhibit the same EDX pattern [44].

The biosynthesized iron oxide nanoparticles' size and crystallinity were also analyzed using XRD. In an XRD analysis, the crystalline nature and plane orientation of FeO NPs were clearly visible. At 2Theta or diffraction angles of 33.15, 24.13, 40.85, 35.612, 49.48, 54.09, 62.41, 57.59, and 63.99 degrees, the most prominent XRD peaks were spotted: 104, 012, 113, 110, 024, 116, 214, and 018. Crystal morphology and an average crystal size of 25-50 nm were confirmed by X-ray diffraction (XRD), which agreed with the International Center for Diffraction Data card (JCPDS-36-1451), confirming the synthesis of an amorphous agglomerated structure, which is consistent with the findings of prior studies [45]

The most significant bactericidal action was seen against *Pseudomonas aeruginosa*, followed by *Proteus vulgaris*, *Escherichia coli*, and *Staphylococcus aureus*. Iron oxide nanoparticles can interact with bacterial cell membranes, causing them to perforate and expel their internal contents into the surrounding media, thus posing a health risk [46]. Absorbance at 260 nm in a membrane damage experiment demonstrated that the concentration of nanoparticles in a culture suspension of *Staphylococcus aureus* increased more damage done to the membrane. At a concentration of 25 g/ml, the A260 for *Staphylococcus aureus* is 32.39±0.15%, at 50 µg/ml, it is 42.47±0.26%, and at a concentration of 100 µg/ml, it is 74.12±0.28%. Specifically, *Pseudomonas aeruginosa* 19.41±0.35%, 27.76±0.55% 45.23±0.22%, 53.51±0.85% The MIC values for iron oxide nanoparticles against *E. coli* are as follows: 53.64±0.56% at 400µg/ml; 21.16±0.24% at 25 µg/ml; 33.29±0.66% at 50 µg/l; 51.86±0.73% at 100 µg/ml; 62.37±0.28% at 200 µg/ml; and 72.1±0.93% at 400 µg/ml. Because of their small size and high concentration, nanoparticles are able to quickly penetrate the bacterial protective walls and cause damage on the inside. This is relevant for their antibacterial, antifungal, and other biological properties [47].

EtBr was used in this essay, instrument-free, agar-based approach to show that bacteria have an efflux pump. This method is a refined and enhanced variant of the EtBr-agar technique reported in [48]. It is a straightforward approach predicated on the substrate specificity of ethidium bromide (EtBr) efflux pumps and the capacity of bacteria to excrete the compound. Efflux pump inhibitors cause EtBr to concentrate inside the cells, where it can trigger blossom at much lower concentrations. The efflux inhibitory effect of iron oxide NPs was assessed using a cart wheel test. we performed cartwheel assay for *Pseudomonas aeruginosa, Staphylococcus aureus, E coli, Citrobacter freundii, Klebsiella penumoniae* and *proteous vulgaris* by incorporating 2mg/ml, 4mg/ml, 6mg/ml, 8mg/ml, 10mg/ml and 12mg/ml of iron oxide NPs in the agar media and evaluating the fluorescence exhibited by EtBr in all the bacteria tested and the result were compared to the previous research.

It has been determined how effective ZnO and Fe-ZnO NPs were at rupturing red blood cells by measuring the amount of haemoglobin released into the plasma during the hemolytic activity [49]. Activity to regulate the hemolytic property of FeO NPs at 37 °C was shown to vary through a wide percentage range from 1.011, 0.899, 0.788, and 0.567. Compared to the positive control (triton x-100), iron oxide NPs showed much lower hemolytic activity. Hemolysis is induced by the NPs because of the enhanced permeability of the cell, allowing for full lysis. Another study found that the safe nature of bio manufactured PbO nanomaterials against red blood cells. This cell lysis led to the generation of free radicals [50].

Methylene blue dye and Phenol red dye's potential photo catalytic degradation is listed as, Initially, dye molecules are adsorbed on the surface of the photo catalyst, which is then bombarded with UV light, causing the

Frontier in Medical & Health Research

ISSN: (e) 3007-1607 (p) 3007-1593

excitation of electrons in the valance band to the conduction band and the creation of holes (h+) in the valance band. After arriving at the photo catalyst's surface, the h+ and e couple will react with adsorbed water molecules, dissolved oxygen, and the surface's hydroxyl groups to generate hydroxyl and superoxide free radicals. According to scheme 1, the h+ ions react with water molecules to form •OH radicals, whereas the e- ions decrease the dissolved oxygen in dye to form the superoxide anion radical O_2•. Upon acquiring the ability to breakdown the dye molecules, these photo generated radicals would do so by creating intermediate intermediates that ultimately break down into CO_2 and water [51].

Conclusions

The synthesized FeO nanoparticles through greener route has crystalline structure with the particle size ranged from 25 to 50 nm. FeO NPs exhibited significant bactericidal action against *Pseudomonas aeruginosa*. FeO NPs were found capable of quickly penetrating to the bacterial protective walls and increased membrane damage was found in *Staphylococcus aureus*. Iron oxide NPs also showed efflux inhibitory effect on the bacterial strains used. Hemolytic assay confirmed that as compared to the positive control (triton x-100), iron oxide NPs showed much lower hemolytic activity. The synthesized NPs can also be used as photo-catalysts in the degradation of Methylene blue and Phenol red dyes. With increase in time duration the rate of degradation also increased. Maximum degradation at 150min for Methylene blue dye and Phenol red dye was 91.1% and 75.02% respectively.

Declarations

Author contributions

FA and AI performed conceptualization, supervision. Salman, AZ, MQ, AK and MT performed formal analysis and investigation, FA and AI performed validation, writing-original draft, visualization. Salman, AZ, MQ, AK and MT perfumed editing and also contributed to formal analysis. FA and AK contributed in the availability of lab facilities.

Conflict of interest

The authors declare that they have no competing interests.

Data availability:

The data will be available upon proper request to the corresponding author

Ethical approval: Human blood was collected from a healthy volunteer and approval was given by the Bacha Khan University Charsadda Ethical Committee.

REFERENCES

Sahoo M, Vishwakarma S, Panigrahi C. Nanotechnology: Current applications and
future scope in food. Food Front. 2021; 2: 3–22.

Dikshit P K, Kumar J, Das A K, et al. Green Synthesis of Metallic Nanoparticles: Applications and Limitations. Catalysts 2021; 11(8): 902.

Anchan S, Pai S, Sridevi H, et al. Biogenic synthesis of ferric oxide nanoparticles using the leaf extract of Peltophorumpter carpum and their catalytic dye degradation potential. Biocatal Agri Biotech 2019; 20: 101251.

Gudkov S V, Burmistrov D E, Serov D A, et al. Do Iron Oxide Nanoparticles Have Significant Antibacterial Properties. Antibiotics, 2021; 10(7): 884.

Dinesh D, Murugan K,Madhiyazhagan P, et al. Mosquitocidal and antibacterial activity of green-synthesized silver nanoparticles from Aloe vera extracts: towards an effective tool against the malaria vector Anopheles stephensi. Parasitol Res 2015;114(4): 1519-1529.

Govindarajan M, Benelli G. A Facile One-Pot Synthesis of Eco-Friendly Nanoparticles Using Carissacarandas: Ovicidal and Larvicidal Potential on Malaria, Dengue and Filariasis Mosquito Vectors. J Cluster Sci 2017; 28(1): 15-36.

Frontier in Medical & Health Research

ISSN: (e) 3007-1607 (p) 3007-1593

Vincent S, Kovendan K, Chandramohan B, et al. Swift fabrication of silver nanoparticles using Bougainvillea glabra: potential against the Japanese encephalitis vector, Culextritaeniorhynchus Giles (Diptera: Culicidae). Cluster Sci. 2017 28(1): 37-58.

Murugan K, Aarthi N, Kovendan K, et al. Mosquitocidal and antiplasmodial activity of Senna occidentalis (Cassiae) and Ocimumbasilicum (Lamiaceae) from Maruthamalai hills against Anopheles stephensi and Plasmodium falciparum. Parasitol Res. 2015;114(10): 3657-3664.

Gupta A, K, Gupta M. Synthesis and surface engineering of iron oxide nanoparticles for biomedical

applications. Biomaterials, 2005;26(18), 3995-4021.

Chourpa I, Douziech-Eyrolles L, Ngaboni-Okassa L, et al. Molecular composition of iron oxide nanoparticles, precursors for

magnetic drug targeting, as characterized by confocal Raman microspectroscopy. Analyst, 2005; 130(10), 1395-1403.

Revia R A, Zhang M. Magnetite nanoparticles for cancer diagnosis, treatment, and treatment monitoring: recent advances. Mater Today, 2016;19(3), 157-168.

Benelli G . Plant-mediated synthesis of nanoparticles: a newer and safer tool against mosquito-borne diseases?. Asian Pac J Trop Biomed. 2016; 6(4), 353-354.

Nasrullah M, Gul F Z, Hanif S, et al. Green and chemical syntheses of CdO NPs: a comparative study for yield attributes, biological characteristics, and toxicity concerns. ACS omega, 2020; 5(11), 5739-5747.

Ali A, Hira Zafar, Haq I, et al. Synthesis, characterization, applications, and challenges of iron oxide nanoparticles. Nanotec Sci Appl. 2016; 9, 49.

Vanlalveni C, Lallianrawna S, Biswas A, et al. Green synthesis of silver nanoparticles using plant extracts and their antimicrobial activities: A review of recent literature. RSC advances, 2021; 11(5), 2804-2837.

Gudkov S V, Burmistrov D E, Serov D A, et al. Do Iron Oxide Nanoparticles Have Significant Antibacterial Properties?. Antibiotics, 2021;10(7), 884.

Hanini A, Schmitt A, Kacem Ket al. Evaluation of iron oxide nanoparticle biocompatibility. Int J Nanomed. 2011;6: 787.

Yiu H H, Pickard M R, Olariu C I, et al. Fe3O4 -PEI-RITC magnetic nanoparticles with imaging and gene transfer capability: Development of a tool for neural cell transplantation therapies. Pharm. Res. 2012; 29, 1328–1343.

Gong Y, Ji Y, Liu F, et al. Cytotoxicity, oxidative stress and inflammation induced by ZnO nanoparticles in endothelial cells: Interaction with palmitate or lipopolysaccharide. J. Appl. Toxicol. 2017; 37: 895–901.

Bai X, Li L, Liu H, et al. Solvothermal synthesis of ZnO nanoparticles and anti-infection application in vivo. ACS Appl. Mater. Interfaces 2015; 7: 1308–1317.

Billings C, Langley M, Warrington G, et al. Magnetic Particle Imaging: Current and Future Applications, Magnetic Nanoparticle Synthesis Methods and Safety Measures. Int J Mol Sci. 2021;22(14): 7651.

Vijayan S R, Santhiyagu P, Ramasamy R, et al. Seaweeds: A resource for marine bionanotechnology. Enzyme Microb. Technol. 2016; 95: 45–57.

Ahmed S, Ahmad M, Swami B L, et al. A review on plants extract mediated synthesis of silver nanoparticles for antimicrobial applications: A green expertise J. Adv. Res. 2016, 7, 17–28. doi.org/10.1016/j.jare.2015.02.007

Naikoo G A, Mustaqeem M, Hassan I U, et al. Bioinspired and green synthesis of nanoparticles from plant extracts with antiviral and antimicrobial properties: A critical review. J Saudi Chem Soc. 2021; 101304.

Frontier in Medical & Health Research

ISSN: (e) 3007-1607 (p) 3007-1593

Karaagac Z. Transfer of hydrophobic colloidal gold nanoparticles to aqueous phase using catecholaminesJ. Mol. Liq. 2020; 315 113796.

Naikoo G A, Mustaqeem M, Hassan I U, et al. Bioinspired and green synthesis of nanoparticles from plant extracts with antiviral and antimicrobial properties: A critical review. J Saudi Chem Soc. 2021;101304.

El-Sherbiny I M, Salih E. Green synthesis of metallic nanoparticles using biopolymers and plant extracts. Green Metal Nanoparticles: Synthesis, Characterization and Their Applications, 2018; 293-319.

Saemi R, Taghavi E, Jafarizadeh-Malmiri H, et al. Fabrication of green ZnO nanoparticles using walnut leaf extract to develop an antibacterial film based on polyethylene–starch–ZnO NPs. Green Process. Synth. 2021;10(1): 112-124.

Varadavenkatesan T, Lyubchik E, Pai S, et al. Photocatalytic degradation of Rhodamine B by zinc oxide nanoparticles synthesized using the leaf extract of Cyanometraramiflora. J. Photochem. Pho tobiol. B, Biol. 2019; 199: 111621.

Salem S S, Fouda A. Green synthesis of metallic nanoparticles and their prospective biotechnological applications: an overview. Biol. Trace Elem. Res. 2021; 199(1), 344-370.

Rene K, Hortense G K, Pascal W, et al.. Activity of aqueous ethanol extract of Euphorbia prostrata ait on Shigelladysenteriae type 1-induced diarrhea in rats. Indian J. Pharmacol. 2007;39(5); 240.

Zahir A A, Chauhan I S, Bagavan A, et al. Green synthesis of silver and titanium dioxide nanoparticles using Euphorbia prostrata extract shows shift from apoptosis to G0/G1 arrest followed by necrotic cell death in Leishmania donovani. Antimicrob. Agents Chemother. 2015; 59(8): 4782-4799.

Rahmat M, Rehman A, Rahmat S, et al. Highly efficient removal of crystal violet dye from water by MnO2 based nanofibrous mesh/photocatalytic process. J. Mater. Res. Technol. 2019; 8(6): 5149-5159.

Jan F A, Ullah R, Ullah N, et al. Exploring the environmental and potential therapeutic applications of Myrtuscommunis L. assisted synthesized zinc oxide (ZnO) and iron doped zinc oxide (Fe-ZnO) nanoparticles. J. Saudi Chem. Soc. 2021; 25(7): 101278.

Mirza A U, Kareem A, Nami S A, et al.Biogenic synthesis of iron oxide nanoparticles using Agrewiaoptiva and Prunuspersica phyto species: characterization, antibacterial and antioxidant activity. J. Photochem. Photobiol. B, Biol. 2018; 185:262-274.

Prem A A). Green synthesis and characterization of iron oxide nanoparticles using Phyllanthusniruri extract. Orient. J. Chem. 2018; 34(5): 2583.

Sathiya C K, and S Akilandeswari. Fabrication and characterization of silver nanoparticles using Delonixelata leaf broth." Spectrochim Acta A Mol Biomol Spectrosc 2014; 128: 337-341.

I Bibi, N Nazar, S Ata, et al.Green synthesis of iron oxide nanoparticles using *pomegranate* seeds extract and photocatalytic activity evaluation for the degradation of textile dy J. Mater. Res. Technol. 2019; 8(6): 6115-6124 (2019)

W Cai, J Wan .Facile synthesis of superparamagnetic magnetite nanoparticles in liquid polyols" J. coll. Inter. Sci. 2007; 305(2): 366-370.

T Wang, X Jin, Z Chen, et al. Green synthesis of Fe nanoparticles using *eucalyptus* leaf extracts for treatment of eutrophic wastewater" Sci. total environ.2014; 466: 210-213.

Ansari M A, Khan H M, Khan A A, et al. Interaction of silver nanoparticles with Escherichia coli and their cell envelope biomolecules. J. Basic Microbiol. 2014; 54 (9): 905–915.

Lok C.-N, Ho C-M, Chen Ret al. Silver nanoparticles: partial oxidation and antibacterial activities. J. Biol. Inorg. Chem. 2007;12 (4): 527–534.

Frontier in Medical & Health Research

ISSN: (e) 3007-1607 (p) 3007-1593

Martins M, Santos B, Martins A, et al. Management Committee Members of Cost B16 European Commission/European Science Foundation: An instrumentfree method for the demonstration of efflux pump activity of bacteria. Vivo, 2006; 20(5):657-664.

Martins M, Couto I, Viveiros M, et al. Identification of efflux-mediated multi-drug resistance in bacterial clinical isolates by two simple methods. In *Antibiotic resistance protocols* 2010; (pp. 143-157). Humana Press.

Jan F A, Ullah R, Ullah N,et al. Exploring the Environmental and Potential Therapeutic Applications of Myrtuscommunis L. assisted synthesized Zinc oxide (ZnO) and Iron doped Zinc oxide (Fe-ZnO) nanoparticles. J. Saudi Chem. Soc. 2021; 101278.

L Sintubin, B De Gusseme, P Van der Meeren, B F Pycke, W Verstraete, N Boon "The antibacterial activity of biogenic silver and its mode of action" Appl. Microbial. Biotechnol., 91(1), 153-162 (2011).

Abdel wahab N A, &Ghoneim A M (2018). Photocatalytic activity of ZnO coated magnetic crosslinked chitosan/polyvinyl alcohol microspheres. *Materials Science and Engineering: B*, *228*, 7-17.

Faisal S, Jan H, Shah S A, Shah S, Khan A, Akbar M T, & Syed S (2021). Green synthesis of zinc oxide (ZnO) nanoparticles using aqueous fruit extracts of Myristicafragrans: their characterizations and biological and environmental applications. *ACS omega*, *6*(14), 9709-9722.

PreediaBabu E, Subastri A, Suyavaran A, Premkumar K, Sujatha V, Aristatile B, &Thirunavukkarasu C (2017). Size dependent uptake and hemolytic effect of zinc oxide nanoparticles on erythrocytes and biomedical potential of ZnO-ferulic acid conjugates. *Scientific reports*, *7*(1), 1-12.

Khalil A T, Ovais M, Ullah I, Ali M, Jan S A, Shinwari Z K, &Maaza M (2020). Bioinspired synthesis of pure massicot phase lead oxide nanoparticles and assessment of their biocompatibility, cytotoxicity and in-vitro biological properties. *Arabian Journal of Chemistry*, *13*(1), 916-931.

Elango G, &Roopan S M (2016). Efficacy of SnO2 nanoparticles toward photocatalytic degradation of methylene blue dye. *Journal of Photochemistry and Photobiology B: Biology*, *155*, 34-38.